

Strange baryon resonance production in $\sqrt{s_{NN}} = 200$ GeV $p + p$ and $Au + Au$ collisions

B.I. Abelev,⁵⁰ M.M. Aggarwal,³⁰ Z. Ahammed,⁴⁵ J. Amonett,²⁰ B.D. Anderson,²⁰ M. Anderson,⁶ D. Arkhipkin,¹³ G.S. Averichev,¹² Y. Bai,²⁸ J. Balewski,¹⁷ O. Barannikova,⁹ L.S. Barnby,² J. Baudot,¹⁸ S. Bekele,²⁹ V.V. Belaga,¹² A. Bellingeri-Laurikainen,⁴⁰ R. Bellwied,⁴⁸ F. Benedosso,²⁸ S. Bhardwaj,³⁵ A. Bhasin,¹⁹ A.K. Bhati,³⁰ H. Bichsel,⁴⁷ J. Bielcik,⁵⁰ J. Bielcikova,⁵⁰ L.C. Bland,³ S-L. Blyth,²² B.E. Bonner,³⁶ M. Botje,²⁸ J. Bouchet,⁴⁰ A.V. Brandin,²⁶ A. Bravar,³ T.P. Burton,² M. Bystersky,¹¹ R.V. Cadman,¹ X.Z. Cai,³⁹ H. Caines,⁵⁰ M. Calderón de la Barca Sánchez,⁶ J. Castillo,²⁸ O. Catu,⁵⁰ D. Cebra,⁶ Z. Chajecski,²⁹ P. Chaloupka,¹¹ S. Chattopadhyay,⁴⁵ H.F. Chen,³⁸ J.H. Chen,³⁹ J. Cheng,⁴³ M. Cherney,¹⁰ A. Chikanian,⁵⁰ W. Christie,³ J.P. Coffin,¹⁸ T.M. Cormier,⁴⁸ M.R. Cosentino,³⁷ J.G. Cramer,⁴⁷ H.J. Crawford,⁵ D. Das,⁴⁵ S. Das,⁴⁵ S. Dash,¹⁵ M. Daugherty,⁴² M.M. de Moura,³⁷ T.G. Dedovich,¹² M. DePhillips,³ A.A. Derevschikov,³² L. Didenko,³ T. Dietel,¹⁴ P. Djawotho,¹⁷ S.M. Dogra,¹⁹ W.J. Dong,⁷ X. Dong,³⁸ J.E. Draper,⁶ F. Du,⁵⁰ V.B. Dunin,¹² J.C. Dunlop,³ M.R. Dutta Mazumdar,⁴⁵ V. Eckardt,²⁴ W.R. Edwards,²² L.G. Efimov,¹² V. Emelianov,²⁶ J. Engelage,⁵ G. Eppley,³⁶ B. Erazmus,⁴⁰ M. Estienne,¹⁸ P. Fachini,³ R. Fatemi,²³ J. Fedorisin,¹² K. Filimonov,²² P. Filip,¹³ E. Finch,⁵⁰ V. Fine,³ Y. Fisyak,³ J. Fu,⁴⁹ C.A. Gagliardi,⁴¹ L. Gaillard,² M.S. Ganti,⁴⁵ L. Gaudichet,⁴⁰ V. Ghazikhanian,⁷ P. Ghosh,⁴⁵ J.E. Gonzalez,⁷ Y.G. Gorbunov,¹⁰ H. Gos,⁴⁶ O. Grebenyuk,²⁸ D. Grosnick,⁴⁴ S.M. Guertin,⁷ K.S.F.F. Guimaraes,³⁷ N. Gupta,¹⁹ T.D. Gutierrez,⁶ B. Haag,⁶ T.J. Hallman,³ A. Hamed,⁴⁸ J.W. Harris,⁵⁰ W. He,¹⁷ M. Heinz,⁵⁰ T.W. Henry,⁴¹ S. Hepplemann,³¹ B. Hippolyte,¹⁸ A. Hirsch,³³ E. Hjort,²² A.M. Hoffman,²³ G.W. Hoffmann,⁴² M.J. Horner,²² H.Z. Huang,⁷ S.L. Huang,³⁸ E.W. Hughes,⁴ T.J. Humanic,²⁹ G. Igo,⁷ P. Jacobs,²² W.W. Jacobs,¹⁷ P. Jakl,¹¹ F. Jia,²¹ H. Jiang,⁷ P.G. Jones,² E.G. Judd,⁵ S. Kabana,⁴⁰ K. Kang,⁴³ J. Kapitan,¹¹ M. Kaplan,⁸ D. Keane,²⁰ A. Kechechyan,¹² V.Yu. Khodyrev,³² B.C. Kim,³⁴ J. Kiryluk,²³ A. Kisiel,⁴⁶ E.M. Kislov,¹² S.R. Klein,²² A. Kocoloski,²³ D.D. Koetke,⁴⁴ T. Kollegger,¹⁴ M. Kopytine,²⁰ L. Kotchenda,²⁶ V. Kouchpil,¹¹ K.L. Kowalik,²² M. Kramer,²⁷ P. Kravtsov,²⁶ V.I. Kravtsov,³² K. Krueger,¹ C. Kuhn,¹⁸ A.I. Kulikov,¹² A. Kumar,³⁰ A.A. Kuznetsov,¹² M.A.C. Lamont,⁵⁰ J.M. Landgraf,³ S. Lange,¹⁴ S. LaPointe,⁴⁸ F. Laue,³ J. Lauret,³ A. Lebedev,³ R. Lednicky,¹³ C-H. Lee,³⁴ S. Lehocka,¹² M.J. LeVine,³ C. Li,³⁸ Q. Li,⁴⁸ Y. Li,⁴³ G. Lin,⁵⁰ X. Lin,⁴⁹ S.J. Lindenbaum,²⁷ M.A. Lisa,²⁹ F. Liu,⁴⁹ H. Liu,³⁸ J. Liu,³⁶ L. Liu,⁴⁹ Z. Liu,⁴⁹ T. Ljubicic,³ W.J. Llope,³⁶ H. Long,⁷ R.S. Longacre,³ W.A. Love,³ Y. Lu,⁴⁹ T. Ludlam,³ D. Lynn,³ G.L. Ma,³⁹ J.G. Ma,⁷ Y.G. Ma,³⁹ D. Magestro,²⁹ D.P. Mahapatra,¹⁵ R. Majka,⁵⁰ L.K. Mangotra,¹⁹ R. Manweiler,⁴⁴ S. Margetis,²⁰ C. Markert,⁴² L. Martin,⁴⁰ H.S. Matis,²² Yu.A. Matulenko,³² C.J. McClain,¹ T.S. McShane,¹⁰ Yu. Melnick,³² A. Meschanin,³² J. Millane,²³ M.L. Miller,²³ N.G. Minaev,³² S. Mioduszewski,⁴¹ C. Mironov,²⁰ A. Mischke,²⁸ D.K. Mishra,¹⁵ J. Mitchell,³⁶ B. Mohanty,⁴⁵ L. Molnar,³³ C.F. Moore,⁴² D.A. Morozov,³² M.G. Munhoz,³⁷ B.K. Nandi,¹⁶ C. Nattrass,⁵⁰ T.K. Nayak,⁴⁵ J.M. Nelson,² P.K. Netrakanti,⁴⁵ L.V. Nogach,³² S.B. Nurushev,³² G. Odyniec,²² A. Ogawa,³ V. Okorokov,²⁶ M. Oldenburg,²² D. Olson,²² M. Pachr,¹¹ S.K. Pal,⁴⁵ Y. Panebratsev,¹² S.Y. Panitkin,³ A.I. Pavlinov,⁴⁸ T. Pawlak,⁴⁶ T. Peitzmann,²⁸ V. Perevoztchikov,³ C. Perkins,⁵ W. Peryt,⁴⁶ S.C. Phatak,¹⁵ R. Picha,⁶ M. Planinic,⁵¹ J. Pluta,⁴⁶ N. Poljak,⁵¹ N. Porile,³³ J. Porter,⁴⁷ A.M. Poskanzer,²² M. Potekhin,³ E. Potrebenikova,¹² B.V.K.S. Potukuchi,¹⁹ D. Prindle,⁴⁷ C. Pruneau,⁴⁸ J. Putschke,²² G. Rakness,³¹ R. Raniwala,³⁵ S. Raniwala,³⁵ R.L. Ray,⁴² S.V. Razin,¹² J. Reinnarth,⁴⁰ D. Relyea,⁴ F. Retiere,²² A. Ridiger,²⁶ H.G. Ritter,²² J.B. Roberts,³⁶ O.V. Rogachevskiy,¹² J.L. Romero,⁶ A. Rose,²² C. Roy,⁴⁰ L. Ruan,²² M.J. Russcher,²⁸ R. Sahoo,¹⁵ T. Sakuma,²³ S. Salur,⁵⁰ J. Sandweiss,⁵⁰ M. Sarsour,⁴¹ P.S. Sazhin,¹² J. Schambach,⁴² R.P. Scharenberg,³³ N. Schmitz,²⁴ K. Schweda,²² J. Seger,¹⁰ I. Selyuzhenkov,⁴⁸ P. Seyboth,²⁴ A. Shabetai,²⁰ E. Shahaliev,¹² M. Shao,³⁸ M. Sharma,³⁰ W.Q. Shen,³⁹ S.S. Shimanskiy,¹² E. Sichtermann,²² F. Simon,²³ R.N. Singaraju,⁴⁵ N. Smirnov,⁵⁰ R. Snellings,²⁸ G. Sood,⁴⁴ P. Sorensen,³ J. Sowinski,¹⁷ J. Speltz,¹⁸ H.M. Spinka,¹ B. Srivastava,³³ A. Stadnik,¹² T.D.S. Stanislaus,⁴⁴ R. Stock,¹⁴ A. Stolpovsky,⁴⁸ M. Strikhanov,²⁶ B. Stringfellow,³³ A.A.P. Suaide,³⁷ E. Sugarbaker,²⁹ M. Sumbera,¹¹ Z. Sun,²¹ B. Surrow,²³ M. Swanger,¹⁰ T.J.M. Symons,²² A. Szanto de Toledo,³⁷ A. Tai,⁷ J. Takahashi,³⁷ A.H. Tang,³ T. Tarnowsky,³³ D. Thein,⁷ J.H. Thomas,²² A.R. Timmins,² S. Timoshenko,²⁶ M. Tokarev,¹² T.A. Trainor,⁴⁷ S. Trentalange,⁷ R.E. Tribble,⁴¹ O.D. Tsai,⁷ J. Ulery,³³ T. Ullrich,³ D.G. Underwood,¹ G. Van Buren,³ N. van der Kolk,²⁸ M. van Leeuwen,²² A.M. Vander Molen,²⁵ R. Varma,¹⁶ I.M. Vasilevski,¹³ A.N. Vasiliev,³² R. Vernet,¹⁸ S.E. Vigdor,¹⁷ Y.P. Viyogi,¹⁵ S. Vokal,¹² S.A. Voloshin,⁴⁸ W.T. Waggoner,¹⁰ F. Wang,³³ G. Wang,⁷ J.S. Wang,²¹ X.L. Wang,³⁸ Y. Wang,⁴³ J.W. Watson,²⁰ J.C. Webb,⁴⁴ G.D. Westfall,²⁵ A. Wetzler,²² C. Whitten Jr.,⁷ H. Wieman,²² S.W. Wissink,¹⁷ R. Witt,⁵⁰ J. Wood,⁷ J. Wu,³⁸ N. Xu,²² Q.H. Xu,²² Z. Xu,³ P. Yepes,³⁶ I-K. Yoo,³⁴ V.I. Yurevich,¹² W. Zhan,²¹ H. Zhang,³ W.M. Zhang,²⁰ Y. Zhang,³⁸ Z.P. Zhang,³⁸ Y. Zhao,³⁸ C. Zhong,³⁹ R. Zoukarnееv,¹³ Y. Zoukarnееva,¹³ A.N. Zubarev,¹² and J.X. Zuo³⁹

(STAR Collaboration)

- ¹Argonne National Laboratory, Argonne, Illinois 60439
²University of Birmingham, Birmingham, United Kingdom
³Brookhaven National Laboratory, Upton, New York 11973
⁴California Institute of Technology, Pasadena, California 91125
⁵University of California, Berkeley, California 94720
⁶University of California, Davis, California 95616
⁷University of California, Los Angeles, California 90095
⁸Carnegie Mellon University, Pittsburgh, Pennsylvania 15213
⁹University of Illinois, Chicago
¹⁰Creighton University, Omaha, Nebraska 68178
¹¹Nuclear Physics Institute AS CR, 250 68 Řež/Prague, Czech Republic
¹²Laboratory for High Energy (JINR), Dubna, Russia
¹³Particle Physics Laboratory (JINR), Dubna, Russia
¹⁴University of Frankfurt, Frankfurt, Germany
¹⁵Institute of Physics, Bhubaneswar 751005, India
¹⁶Indian Institute of Technology, Mumbai, India
¹⁷Indiana University, Bloomington, Indiana 47408
¹⁸Institut de Recherches Subatomiques, Strasbourg, France
¹⁹University of Jammu, Jammu 180001, India
²⁰Kent State University, Kent, Ohio 44242
²¹Institute of Modern Physics, Lanzhou, China
²²Lawrence Berkeley National Laboratory, Berkeley, California 94720
²³Massachusetts Institute of Technology, Cambridge, MA 02139-4307
²⁴Max-Planck-Institut für Physik, Munich, Germany
²⁵Michigan State University, East Lansing, Michigan 48824
²⁶Moscow Engineering Physics Institute, Moscow Russia
²⁷City College of New York, New York City, New York 10031
²⁸NIKHEF and Utrecht University, Amsterdam, The Netherlands
²⁹Ohio State University, Columbus, Ohio 43210
³⁰Panjab University, Chandigarh 160014, India
³¹Pennsylvania State University, University Park, Pennsylvania 16802
³²Institute of High Energy Physics, Protvino, Russia
³³Purdue University, West Lafayette, Indiana 47907
³⁴Pusan National University, Pusan, Republic of Korea
³⁵University of Rajasthan, Jaipur 302004, India
³⁶Rice University, Houston, Texas 77251
³⁷Universidade de Sao Paulo, Sao Paulo, Brazil
³⁸University of Science & Technology of China, Hefei 230026, China
³⁹Shanghai Institute of Applied Physics, Shanghai 201800, China
⁴⁰SUBATECH, Nantes, France
⁴¹Texas A&M University, College Station, Texas 77843
⁴²University of Texas, Austin, Texas 78712
⁴³Tsinghua University, Beijing 100084, China
⁴⁴Valparaiso University, Valparaiso, Indiana 46383
⁴⁵Variable Energy Cyclotron Centre, Kolkata 700064, India
⁴⁶Warsaw University of Technology, Warsaw, Poland
⁴⁷University of Washington, Seattle, Washington 98195
⁴⁸Wayne State University, Detroit, Michigan 48201
⁴⁹Institute of Particle Physics, CCNU (HZNU), Wuhan 430079, China
⁵⁰Yale University, New Haven, Connecticut 06520
⁵¹University of Zagreb, Zagreb, HR-10002, Croatia

(Dated: October 29, 2018)

We report the measurements of $\Sigma(1385)$ and $\Lambda(1520)$ production in $p + p$ and $Au + Au$ collisions at $\sqrt{s_{NN}} = 200$ GeV from the STAR collaboration. The yields and the p_T spectra are presented and discussed in terms of chemical and thermal freeze-out conditions and compared to model predictions. Thermal and microscopic models do not adequately describe the yields of all the resonances produced in central $Au + Au$ collisions. Our results indicate that there may be a time-span between chemical and thermal freeze-out during which elastic hadronic interactions occur.

PACS numbers:

In ultra-relativistic heavy ion collisions, hot and dense nuclear matter (a fireball) is created [1, 2]. When the

energy density of the created fireball is very high, deconfinement of partons is expected to occur and a new phase of matter, the Quark Gluon Plasma (QGP) forms. After hadronization of the QGP, but before the interactions of the hadrons cease, the physical properties of resonances, such as their in vacuo masses and widths, might be modified by the density of the surrounding nuclear medium [3]. In addition, the yield of resonances might change.

The temperature and the density of the fireball reduces as the fireball expands. Chemical freeze-out is reached when hadrons stop interacting inelastically. Elastic interactions continue until thermal freeze-out. Due to their short lifetimes, a fraction of resonances can decay before the thermal freeze-out. Elastic interactions of the decay products with other particles in the medium (re-scattering) may modify their momenta enough that the parent particle can no longer be identified. The pseudo-elastic hadronic interactions (regeneration) may increase the resonance yields (e.g., $\Lambda + \pi \rightarrow \Sigma(1385)$) [4, 5, 6, 7]. The overall net effect of re-scattering and regeneration on the total observed yields depends on the time-span between chemical and thermal freeze-out, the lifetime of the resonances and the magnitudes of the interaction cross-sections of the decay particles [8, 9]. Thermal models provide the resonance to stable particle ratios at the chemical freeze-out. Deviations from these predicted ratios due to re-scattering of the resonance decay particles can be used to estimate the time-span between chemical and thermal freeze-out.

We report on the first measurements of the production of the $\Sigma(1385)$ [10] and $\Lambda(1520)$ [11] in $p + p$ and $Au + Au$ collisions at $\sqrt{s_{NN}} = 200$ GeV. The effects of the extended nuclear medium on the resonance yields and momentum spectra are studied by comparing those results from the different collision systems. Microscopic transport [4] and thermal [12, 13, 14] models are used to investigate the time-span of hadronically interacting phase.

The STAR detector system [15], with its large time projection chamber (TPC), is used to identify the decay products of the $\Sigma(1385) \rightarrow \Lambda + \pi$ and $\Lambda(1520) \rightarrow p + K$. For $Au + Au$ collisions, the number of charged particles in the TPC is used to select the centrality of inelastic interactions. Different y and centrality selections are necessary for $\Sigma(1385)$ and $\Lambda(1520)$ in order to optimize the statistical significance of each measurement.

The topological reconstruction of resonance decay vertices is not possible due to their short lifetimes resulting from their strong decay. Instead an invariant mass calculation from the decay daughter candidates is performed. Charged particles are identified by the energy loss per unit length, dE/dx , and the momentum measured with the TPC. The decay topology information is used to identify the neutral Λ [16]. A large source of background in the invariant mass spectra for both $\Sigma(1385)$ and $\Lambda(1520)$ comes from uncorrelated pairs. A mixed event technique, where no correlations are possible, is used to estimate the contribution of the background [17]. The background is

normalized over a wide kinematic range and then subtracted from the invariant mass distribution. For the $\Sigma^-(1385)$, a Ξ^- peak remains as it has the same $\Lambda + \pi^-$ decay channel. In order to enhance the statistics for the Σ^* , two charged channels are combined ($\Sigma^\pm(1385)$) for $p+p$ and all four charged channels ($\Sigma^\pm(1385) + \bar{\Sigma}^\pm(1385)$) for $Au + Au$ collisions. Similarly for the Λ^* , $\Lambda(1520)$ and $\bar{\Lambda}(1520)$ are combined in $p + p$ collisions. As the $\bar{\Lambda}(1520)$ is not observed in central $Au + Au$ collisions, it is not included in our definition of Λ^* in $Au + Au$.

Fig. 1 shows the invariant mass distributions for Σ^* and Λ^* in 10 million minimum bias $p + p$ and 1.6 million central $Au + Au$ collisions. The mass (M) and the width (Γ) fit parameters of the measured transverse momentum (p_T) and rapidity (y) ranges are shown in Table I.

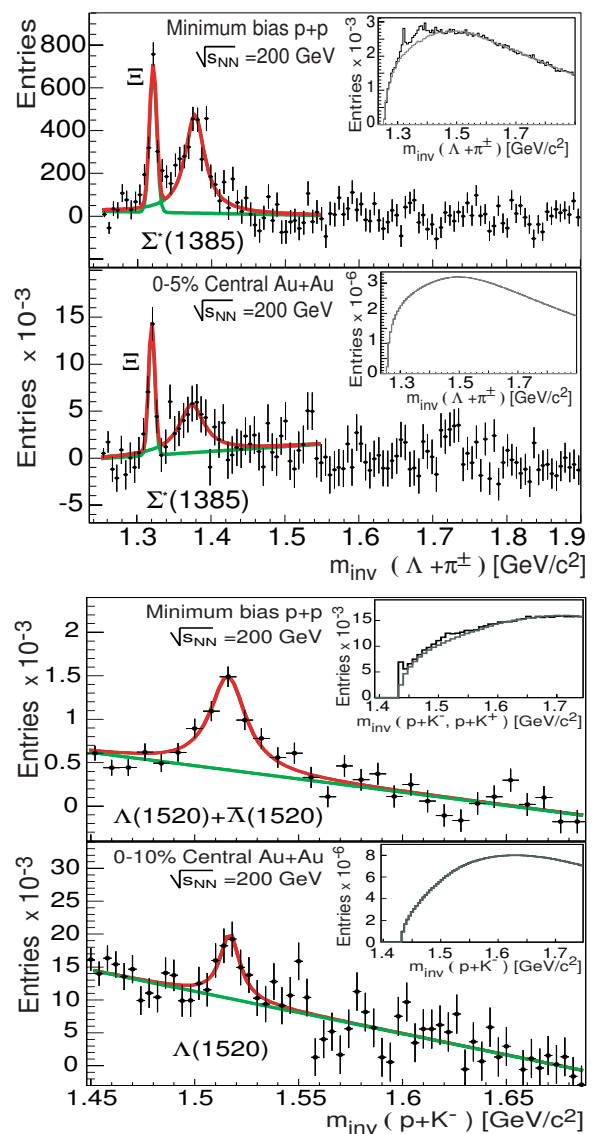


FIG. 1: Invariant mass distributions of Σ^* and Λ^* in $p + p$ and $Au + Au$ collisions at $\sqrt{s_{NN}} = 200$ GeV before (inset) and after mixed-event background subtraction.

These parameters and their uncertainties are obtained from combined fits. A Gaussian distribution takes into account the detector resolution effects on the Ξ^- . Since the natural width dominates over the detector resolutions for both the Σ^* and Λ^* , a non-relativistic Breit-Wigner distribution is used. Finally the remaining residual background is described by a linear function. The measured widths, taking into account the detector resolution, are, within their uncertainties, in agreement with the PDG [18]. The observed mass and the width of the Ξ^- peak is in agreement with the one obtained via the topological method [16]. While the masses of Ξ and Λ^* are also in agreement with the PDG values, there is a small difference in the mass of the Σ^* . Due to limited statistics, it is not possible to investigate this effect further. The systematic errors include the uncertainty due to bin size fluctuations, the normalization of the mixed event background and the uncertainty of the straight line fit range due to correlations in misidentified decay particles. Event and track selections were also varied.

To obtain the integrated raw yields of Σ^* and Λ^* , the background subtracted invariant mass spectrum in each p_T bin is fitted. In the corresponding mass range, the content of each bin above the linear background fit is counted to extract the raw yields. Monte-Carlo simulated resonances are embedded into real $p+p$ and $Au+Au$ events to determine the correction factors for the detector acceptance and reconstruction efficiency. These are applied to the data and the corrected transverse mass spectra of Σ^* and Λ^* in $p+p$ and $Au+Au$ collisions are shown in Fig. 2. The dashed curves represent an exponential fit to the data [17]. The mean p_T ($\langle p_T \rangle$) and the yields at mid-rapidity (dN/dy) as obtained from the fit are listed in Table II together with their corresponding statistical uncertainties. The yields are obtained by extrapolating the fit to all p_T . The measured p_T range contains 85% for Σ^* and 50% for Λ^* in $Au+Au$ and 91% for Σ^* and Λ^* in $p+p$ of the total mid-rapidity yields. For Λ^* , due to the low statistics in $Au+Au$ collisions, an inverse slope of $T = 400$ MeV is assumed in order to extract the particle yield. The systematic error includes a $\Delta T = 100$ MeV variation. The ratio of $\bar{\Lambda}^*/\Lambda^* = 0.93 \pm 0.11$ in $p+p$ collisions is extracted from the corrected yields. Statistical limitations require that the $\bar{\Sigma}^*/\Sigma^* = 0.87 \pm 0.18$ in

TABLE I: Mass (M) and width (Γ) fit parameters of particles from Fig. 1, including statistical and systematic errors.

Particle	M [MeV/c ²]	Γ [MeV/c ²]	p_T [GeV/c]	$ y $
$\Xi^-_{(p+p)}$	$1320 \pm 1 \pm 1$	$7 \pm 1 \pm 1$	0.25 - 3.50	≤ 0.75
$\Xi^-_{(Au+Au)}$	$1320 \pm 1 \pm 1$	$4 \pm 1 \pm 1$	0.50 - 3.50	≤ 0.75
$\Sigma^*_{(p+p)}$	$1376 \pm 3 \pm 3$	$44 \pm 8 \pm 8$	0.25 - 3.50	≤ 0.75
$\Sigma^*_{(Au+Au)}$	$1375 \pm 5 \pm 3$	$43 \pm 5 \pm 6$	0.50 - 3.50	≤ 0.75
$\Lambda^*_{(p+p)}$	$1516 \pm 2 \pm 2$	$20 \pm 4 \pm 2$	0.20 - 2.20	≤ 0.50
$\Lambda^*_{(Au+Au)}$	$1516 \pm 2 \pm 2$	$12 \pm 6 \pm 3$	0.90 - 2.00	≤ 1.00

TABLE II: $\langle p_T \rangle$ and yields from fits to the p_T spectra, dN/dy for Λ^* in $Au+Au$ using a fixed T . The $p+p$ yields are from non-singly diffractive collisions. Σ^* represents $\Sigma^{*+} + \Sigma^{*-}$.

Particle	Collision	$\langle p_T \rangle$ [GeV/c]	$(dN/dy) _{y=0}$
Σ^*	$pp_{minbias}$	$1.02 \pm 0.02 \pm 0.07$	$(10.7 \pm 0.4 \pm 1.4) \times 10^{-3}$
$\bar{\Sigma}^*$	$pp_{minbias}$	$1.01 \pm 0.01 \pm 0.06$	$(8.9 \pm 0.4 \pm 1.2) \times 10^{-3}$
$\bar{\Sigma}^* + \Sigma^*$	$AuAu_{0-5\%}$	$1.28 \pm 0.15 \pm 0.09$	$9.3 \pm 1.4 \pm 1.2$
$\bar{\Lambda}^* + \Lambda^*$	$pp_{minbias}$	$1.08 \pm 0.09 \pm 0.05$	$(6.9 \pm 0.5 \pm 1.0) \times 10^{-3}$
Λ^*	$AuAu_{0-10\%}$	$1.20 \pm 0.20_{fixed}$	$(6.3 \pm 2.1 \pm 0.8) \times 10^{-1}$
$\bar{\Lambda}^* + \Lambda^*$	$AuAu_{60-80\%}$	$1.20 \pm 0.20_{fixed}$	$(8.9 \pm 2.9 \pm 1.1) \times 10^{-2}$

$Au+Au$ collisions are determined from the raw yields. The proximity of these ratios to unity, reflects a small net baryon number at mid-rapidity of both systems.

A linear increase of $\langle p_T \rangle$ as a function of particle mass up to 1 GeV/c² is observed in $Au+Au$ and $p+p$ collisions [16, 19]. The measured $\langle p_T \rangle$ of Σ^* and Λ^* in $p+p$ collisions follow a steeper increase, similar to the trend of heavier mass particles (> 1 GeV/c²). This might be due to the fact that the higher mass particles come from events with average multiplicities a factor of 2 or more higher than those for the minimum bias events. The increase in the $\langle p_T \rangle$ and the larger event multiplicities imply that these resonances come from mini-jet like events [20]. The re-scattering and regeneration is expected to change the $\langle p_T \rangle$ in $Au+Au$ collisions. However, it is surprising that the $\langle p_T \rangle$ of Σ^* in $p+p$ and $Au+Au$ collisions are in agreement within their uncertainties.

The ratios of yields of resonances to stable particles as a function of the charged particle multiplicity are presented in Fig. 3. The ratios are normalized to unity in $p+p$ collisions to study variations in $Au+Au$ relative to $p+p$. We measure a suppression for Λ^*/Λ when comparing central $Au+Au$ with minimum bias $p+p$. K^*/K^- [17] seems to show a smaller suppression while the Σ^*/Λ , and ϕ/K^- [21] ratios are consistent with unity. In a

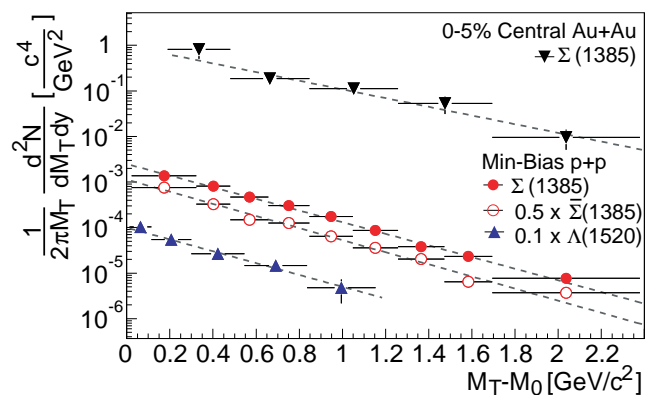


FIG. 2: The transverse mass spectra for Σ^* and Λ^* in $p+p$ and in central $Au+Au$ collisions at $\sqrt{s_{NN}} = 200$ GeV. Statistical and systematic errors are included.

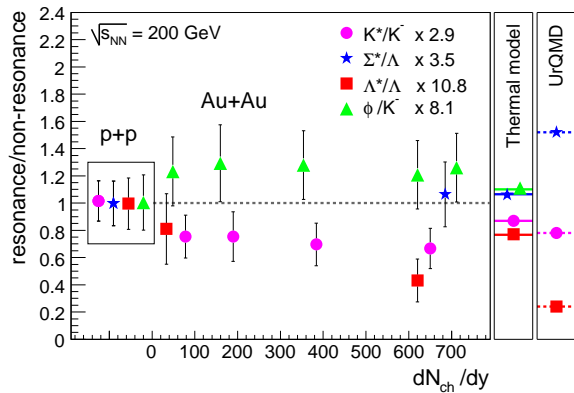


FIG. 3: Resonance to stable particle ratios for $p + p$ and $Au + Au$ collisions. The ratios are normalized to unity in $p + p$ and compared to thermal and UrQMD model predictions for central $Au + Au$ [8, 12]. Statistical and systematic uncertainties are included in the error bars.

thermal model, the measured ratios of resonance to non-resonant particles with identical valence quarks are particularly sensitive to the chemical freeze-out temperature, as all of the quark content dependencies cancel out. Thermal models require a chemical freeze-out temperature in the range $T = 160 - 180$ MeV and a baryo-chemical potential $\mu_B = 20 - 50$ MeV in 200 GeV $Au + Au$ collisions to describe the stable particle ratios [12, 13]. While these models predict the measured Σ^*/Λ ratio correctly within the errors, they yield a higher ratio than the measured Λ^*/Λ in the most central $Au + Au$ collisions. This suggests an extended hadronic phase of elastic and pseudo-elastic interactions after chemical freeze-out, where re-scattering of resonance decay particles and regeneration of resonances will occur. The measured resonance yields thus depend on the time-span between chemical and kinetic freeze-out, their cross sections for re-scattering and regeneration, and their lifetimes. The suppressed Λ^*/Λ and K^*/K^- ratios in $Au + Au$ suggest that re-scattering dominates regeneration in the hadronic medium after chemical freeze-out.

A thermal model using an additional pure re-scattering phase, which depends on the respective momenta of the resonance decay products, after chemical freeze-out at $T = 160$ MeV, can be fit to the data [9, 22]. The fit yields a hadronic lifetime of the source of $\Delta\tau = 9^{+10}_{-5}$ fm/c from the Λ^*/Λ and $\Delta\tau = 2.5^{+1.5}_{-1}$ fm/c from the K^*/K^- ratio. The small difference between the time spans can be explained by an enhanced regeneration cross section for the K^* in the medium. This theory is supported by the null suppression of the Σ^*/Λ . The smaller lifetime of the Σ^* compared to the Λ^* should lead to a larger signal loss due to re-scattering, thus the lack of suppression requires an enhanced regeneration probability of the Σ^* . Based on the same argument the K^* regeneration cross section needs to be larger than that of the Λ^* due to the observed smaller suppression and shorter lifetime of the K^* (i.e., defining R as the ratio of regeneration to re-

scattering cross section, we find $R_{K+p} < R_{K+\pi} < R_{\Lambda+\pi}$ since $c\tau_{K^*} < c\tau_{\Sigma^*} < c\tau_{\Lambda^*}$). A microscopic model calculation (UrQMD) with a typical lifespan of $\Delta\tau = 13 \pm 3$ fm/c for the re-scattering and regeneration phase, can describe K^*/K^- and Λ^*/Λ ratios approximately, but fails for the Σ^*/Λ [8]. The measured resonance yields in heavy-ion collisions provide a tool to determine the strength of in-medium hadronic cross sections and current microscopic transport models such as UrQMD will have to be modified to account for such cross sections [23]. The $\Delta\tau$ extracted from the measurements can be used in comparison to the analysis of two-pion intensity interferometry (HBT) in order to obtain an estimate for the partonic lifetime. Identical particle HBT yields a time of 5-12 fm/c from the start of the collision to the kinetic freeze-out (total source lifetime) [24]. If one assumes the Λ^* to be least affected by regeneration then the extracted $\Delta\tau > 4$ fm/c is a lower limit on the hadronic source lifetime, which is a sub-interval of the total source lifetime. The remaining time would be a rough estimate on the partonic lifetime of the source.

Although the re-scattering and regeneration scheme is discussed predominantly, other methods to describe the data have been proposed. For example, in a sudden freeze-out scenario, where the time between the chemical and kinetic freeze-out is negligible, the Λ^*/Λ suppression in $Au + Au$ with respect to $p + p$ can be explained by the influence of the dense medium on the production of Λ^* . Even though the valence quarks of the Λ^* are in a $L = 1^-$ state, it must decay through a relative angular momentum $L = 2$ process in order to conserve isospin [25]. The high partial wave component of the Λ^* in a dense medium can suppress its decay phase space.

We have presented the first measurements of Σ^* and Λ^* production in $p + p$ and $Au + Au$ collisions at $\sqrt{s_{NN}} = 200$ GeV. The large $\langle p_T \rangle$ of the Σ^* and Λ^* measurements in $p + p$ collisions suggests that the heavy particle production receives a significant contribution from jet-like events. The yields of Σ^* , Λ^* , ϕ and K^* in $Au + Au$ in comparison to $p + p$ collisions indicate the presence of re-scattering and regeneration for a non-zero time-span between chemical and kinetic freeze-out. A lower limit for the hadronic source lifetime of $\Delta\tau > 4$ fm/c is estimated based on a thermal model including re-scattering.

We thank the RHIC Operations Group and RCF at BNL, and the NERSC Center at LBNL for their support. This work was supported in part by the Offices of NP and HEP within the U.S. DOE Office of Science; the U.S. NSF; the BMBF of Germany; IN2P3, RA, RPL, and EMN of France; EPSRC of the United Kingdom; FAPESP of Brazil; the Russian Ministry of Science and Technology; the Ministry of Education and the NNSFC of China; IRP and GA of the Czech Republic, FOM of the Netherlands, DAE, DST, and CSIR of the Government of India; Swiss NSF; the Polish State Committee for Scientific Research; SRDA of Slovakia, and the Korea Sci. & Eng. Foundation.

-
- [1] K. Adcox *et al.*, Phys. Rev. Lett. **87**, 052301 (2001).
[2] J. Adams *et al.*, Phys. Rev. Lett. **92**, 112301 (2004).
[3] M.F.M. Lutz *et al.*, Nucl. Phys. **A700**, 193 (2002).
[4] S.A. Bass *et al.*, Phys. Rev. **C61**, 064909 (2000).
[5] R. Rapp *et al.*, Phys. Rev. Lett. **86**, 2980 (2001).
[6] H. van Hees *et al.*, Phys. Lett. **B606** 59 (2005).
[7] C. Adler *et al.*, Phys. Rev. **C66**, 061901 (2002).
[8] M. Bleicher *et al.*, Phys. Lett. **B530**, 81 (2002);
M. Bleicher, Nucl. Phys. **A715**, 85 (2003).
[9] G. Torrieri *et al.*, Phys. Lett. **B509**, 239 (2001);
J. Rafelski *et al.*, Phys. Rev. **C64**, 054907 (2001);
J. Rafelski *et al.*, Phys. Rev. **C65**, 069902,(2002).
[10] S. Salur, PhD Thesis, Yale University, May 2006.
[11] L. Gaudichet, PhD Thesis, Nantes University, Oct 2003.
[12] P. Braun-Munzinger *et al.* Phys. Lett. **B518**, 41 (2001).
[13] F. Becattini, Nucl. Phys. **A702**, 336 (2002).
[14] J. Adams *et al.*, Nucl. Phys. **A 757** 102 (2005).
[15] M. Anderson *et al.*, Nucl. Inst. Meth. **A499**, 659 (2003).
[16] B. Ablev *et al.*, nucl-ex/0601042.
[17] J. Adams *et al.*, Phys. Rev. **C71**, 064902 (2005).
[18] S. Eidelman *et al.*, Phys. Lett. **B592**, (2004).
[19] B. Ablev *et al.*, nucl-ex/0607033.
[20] A. Dumitru *et al.*, Phys. Lett. **B446**, 326 (1999).
[21] J. Adams *et al.*, Phys. Lett. **B612**, 181 (2005).
[22] C. Markert *et al.*, hep-ph/0206260.
[23] S. Vogel *et al.*, hep-ph/0607242.
[24] J. Adams *et al.*, Phys. Rev. **C71**, 044906 (2005).
[25] M. Kaskulov *et al.*, nucl-th/0509088.